processes

MDPI

Article

Study on Mechanism and Regularity of Rock Breaking by Pulsed Water Injection with Particles

Tian Zhao [1], Qingxiang Wu [2], Haifeng Lv [2], Heng Song [1], Xinke Yang [1] and Tiancheng Fang [3,*]

[1] Engineering Technology Research Institute of Petro China Xinjiang Oilfield Company (Supervision Company), Karamay 834000, China; songheng39@petrochina.com.cn (H.S.)
[2] Development Department of Petro China Xinjiang Oilfield Company, Karamay 834000, China
[3] Northeast Petroleum University, Daqing 163318, China
* Correspondence: fangtc211@163.com

Abstract: In recent years, the drilling technology applied to deep and ultra-deep formations has developed rapidly, but the drilling speed for hard formations is low. Therefore, it is very important to study the drilling methods for deep and hard strata. Particle pulsed jet drilling is a new drilling method based on particle jet impact drilling technology and high-pressure pulsed water jet impact drilling technology. In this paper, the mathematical models of the shear layer amplification coefficient and wave velocity are established based on a similar network theory, and the motion equations of a single particle and particle swarm are established according to the motion of particles in a pulsed jet environment. Then, based on the self-designed particle jet impact rock-breaking experimental platform, the numerical simulation results are compared, analyzed, and verified. The results show that the rock-breaking efficiency increases with the increase in the average velocity of the particle pulsed jet. When the average speed exceeds 160 m/s, the rock-breaking efficiency increases significantly. With the increase in the particle concentration, the rock-breaking efficiency of the particle pulsed jet also increases, but there is an optimal value. When the concentration is too high, the impact of particles on the rock is affected by the collision between particles, and the wear of the drill intensifies. This research is helpful for understanding deep-well drilling-speed-increasing technology and promotes the development and engineering applications of particle jet impact drilling theory.

Keywords: particles; rock breaking; pulse; water injection; hard formation; rock drilling

Citation: Zhao, T.; Wu, Q.; Lv, H.; Song, H.; Yang, X.; Fang, T. Study on Mechanism and Regularity of Rock Breaking by Pulsed Water Injection with Particles. *Processes* **2023**, *11*, 2765. https://doi.org/10.3390/pr11092765

Academic Editors: Alberto Di Renzo and Youguo Yan

Received: 17 July 2023
Revised: 3 September 2023
Accepted: 14 September 2023
Published: 15 September 2023

1. Introduction

With the intensification of the exploitation of global shallow oil and gas resources, oil and gas resources in deep and hard formations have gradually become the focus of exploration and development [1,2]. For the development of global deep-well drilling, the first deep, ultra-deep, and extra-deep wells in the world were drilled to depths of 4573 m, 6225 m, and 9159 m, each of which were completed by the United States, and the world's deepest oil-drilling record is a depth of 15,000 m, corresponding to a well in the Odoputu oilfield [3]. At present, with the discovery of a number of large deep and ultra-deep oil and gas fields in the Tarim Basin [4], the Sichuan Basin, and the Junggar Basin [5], the efficient development of deep and ultra-deep oil and gas resources has been set as the focus for the next few years [6]. In recent years, the drilling and completion technology of deep and ultra-deep oil and gas resource development in China have developed rapidly. For example, in 2019, the deepest well, with a depth of 8882 m, was drilled in Asia, indicating that China has basically mastered the drilling and completion technology for 8000 m onshore oil and gas wells [7,8]. However, drilling technology still faces many challenges, as shown in Figure 1, making deep-well and hard-formation drilling internationally recognized drilling problems [1,9].

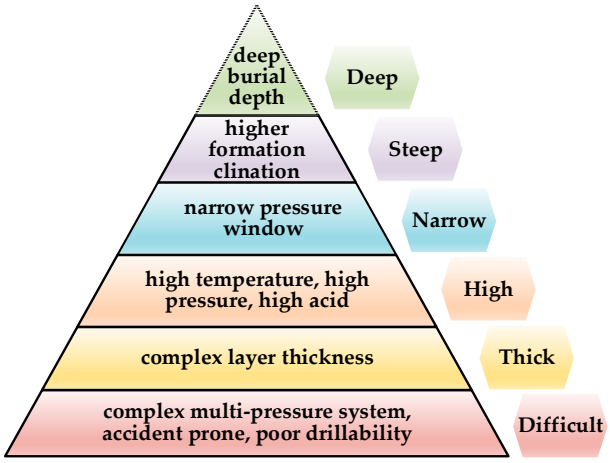

Figure 1. Drilling and completion technology challenges.

Deep and ultra-deep rock have a compact texture, high wear resistance, and high compressive strength, thus aggravating the wear of the bit, reducing drilling efficiency, and seriously restricting the speed and cost of oil and gas exploration and development. With the development of modern science and technology, some new rock-breaking technologies have emerged. Examples include plasma rock-breaking [10,11], microwave rock-breaking [12,13], rotary percussion drilling [14,15], laser drilling [16,17], and other rock-breaking methods [18]. However, in addition to the shortcomings shown in Table 1, a lot of energy is required from the bottom of the hole or the ground to maintain drilling, and recently, the engine power, cable transmission efficiency, underground equipment anti-electromagnetic interference, and other capabilities have begun adding to these high requirements. High-speed water jets fired at rocks cause erosion, and this is also a major process in non-traditional drilling and cutting methods such as hydraulic blasting, hydraulic fracturing, and cavitation drilling. Rock failure morphology under the action of a water jet at different speeds varies greatly, so we can greatly improve rock-breaking efficiency. This is also a widely used drilling method at present. However, this technique's rock-breaking efficiency lags behind some new drilling techniques proposed in recent years. Therefore, the complex and severe working environment in a well limits the application of the above rock-breaking technology. In summary, particle pulsed jet drilling technology is the most widely used, has high rock-breaking efficiency, and has broad prospects for development.

Table 1. Advantages and disadvantages of new rock-breaking technology.

Name	Advantages	Shortcomings
Laser [16,17]	Low cost, high efficiency, low pollution	Use of high power is limited
Plasma [10,11]	Higher rate of penetration	Large energy consumption
Microwave [12,13]	Fast heating, strong penetration, and easy process control	It takes some time for the radiation to take effect
Rotary percussion drilling [14,15]	High stability and drilling efficiency	High pressure resistance of drill bit is required
Water jet [19,20]	Improves rate of penetration and bottom-hole purification effect, reduces rock-holding effect and avoids repeated drill bit damage,	High power consumption and short nozzle life
Particle jet [21–23]	High drilling efficiency, entering the commercial application stage	Steel particle recovery is too complex

In 2002, American engineers Curlett HB, Sharp DP, and Gregory MA were inspired by the idea of "projectile impact rock breaking", so they mixed particles with drilling fluids,

proposed "particle impact rock breaking drilling", and then established the Particle Impact Drilling Company (PDTI) [24,25]. The particle jet drilling system developed by the PDTI company applies particle jet impact drilling technology to the field of drilling engineering. In this setting, hard, spherical metal particles are mixed with drilling fluid. Through the acceleration process of applying drilling fluid to metal particles, high-impact velocity is achieved, and this breaks the rock. A series of experiments conducted in the USA and China have proved that the drilling speed of a particle jet is 3–4-fold greater than that of traditional methods [26,27]. Foreman et al. studied rock failure theory in relation to particle jet impact by using the Griffith rock failure criterion and elastic mechanics theory, and the results obtained showed that the combined effect of the stress wave generated by the particles impacting the rock and the "water wedge effect" of a high-pressure water jet was the main causes of rock breakage [28]. Ai et al. used the JH-2 model to describe brittle materials and simulated the impact process of different particle concentrations at the same impact velocity. Their research showed that the prediction of the damage range inside the rock and the calculation of crack growth could be achieved through the calculation of strength, pressure, and damage data [29]. Cheng mainly analyzed the effect of a particle jet's impact on rock breaking according to three aspects: theoretical research, numerical simulation, and experimental research. The particle volume, impact velocity, incident angle, and other influencing factors in the whole process of particle jet rock breaking were obtained based on the software Fluent and LS DYNA [30]. Zhu et al. established a numerical model of black sandstone by using the discrete-element particle flow method and studied the rock breaking laws of a single particle jet, a multi-particle jet, and assisted cutting under different particle sizes, incident angles, incident velocities, and other factors considering the proportion of the mineral components of black sandstone [21]. Regarding the preliminary research of our team, the SPH and FEM coupled algorithm was used to model the whole process of a particle-slurry's impact on rock breaking, and we mainly studied the influence of the impact velocity, angle, and particle size on rock-breaking efficiency [31,32]. Moreover, the damage mechanisms of rock under a particle-slurry jet were also studied [33]. The above research mainly focuses on the field of particle jet impact rock breaking, and further research is needed on the combination of particle impact and a pulse jet.

This article achieves the goal of particle pulsed jet rock breaking by accelerating the oscillation of drilling fluid and particles using a self-excited oscillation pulse generator and then accelerating it again through a nozzle. This technology is not only suitable for the difficult rock-breaking environment in deep and ultra-deep wells but also greatly reduces drilling costs on the basis of improving drilling efficiency. The cleaning efficiency regarding rock debris and particles is also greatly improved due to the pulse effect. Research on pulsed jets shows that the peak pressure generated by a self-oscillating pulsed jet is 1.5–2.5 times that of a continuous jet [21,26]. However, there is still a lack of research on the factors affecting the efficiency of particle pulsed jet rock breaking.

In this paper, the mechanism and behavior of rock breaking via particle pulsed jet are researched and revealed through experimental and numerical simulation methods. The research process is as follows: Firstly, a mathematical model of the shear layer amplification coefficient and wave velocity is established, and the single particle motion equation and a particle swarm motion equation are also established according to the particle motion in the pulsed water jet environment in order to elucidate the dynamic characteristics of particles in the process of applying a particle pulsed jet. Then, the numerical simulation results are compared with the experimental results and verified based on the self-designed experimental platform for particle jet impact rock breaking to analyze the effect of different parameters on rock-breaking efficiency. This research will help deepen the understanding of particle pulsed jet-drilling technology and promote the development and engineering application of this technology.

2. Mathematical Model

Particle pulsed jet drilling technology is a new rock-breaking technology based on particle jet rock-breaking technology and high-pressure pulsed water jet rock-breaking technology. In particle pulsed jet drilling, a certain proportion of hard particles is added into the original high-pressure drilling fluid. Then, a pulsed jet is formed using an oscillating chamber. The hard particles attain a subsonic speed and inflict stress damage on the rock before drilling using energy fluctuations. As the internal stress of the rock is released, the rock-breaking strength is reduced, and the service life of the equipment used is increased.

The main principle of particle pulsed water jet impact rock breaking is shown in Figure 2. During this process, metal particles are injected into high-pressure water in a fixed proportion by some means, and then the uniform mixture of metal and water generates a high-speed pulsed jet of water and particles via a special vibration cavity. Subsequently, the particle pulsed jet drill makes contact with the rock to break it and thus achieve efficient rock breaking.

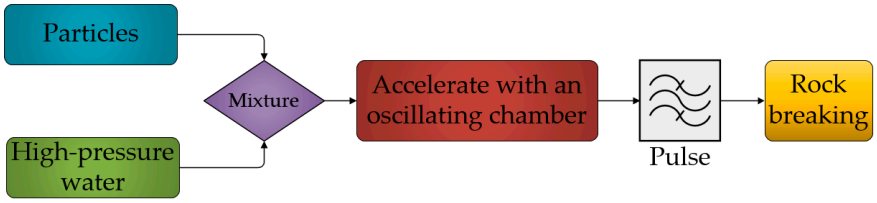

Figure 2. Principle process of particle pulsed jet rock breaking.

The principle of a particle pulsed jet oscillating cavity is shown in Figure 3a, and its three-dimensional structure is shown in Figure 3b. The stable high-pressure mixed flow of particles and water enters the Helmholtz oscillation chamber from the inlet nozzle. After the disturbance wave amplified by the velocity shear layer collides with the impact wall, a "pressure transient" will occur because the area of the mixed flow at the wall is larger than the cross-sectional area of the outlet nozzle. At the same time, the outlet nozzle generates a pressure pulse, and the pressure transient is reflected upstream along the axis at the speed of sound. A pressure transient is generated again at the inlet nozzle, causing the inlet flow to oscillate. The flow contains low-frequency and axisymmetric vortex ring disturbances. Because the velocity shear layer amplifies the vortex rings of different frequencies in different degrees, strong disturbances are generated. These disturbances move towards the outlet with the velocity shear layer and produce pressure transients after colliding with the impact wall. This transient is reflected upstream again to generate positive feedback, which produces a pulse effect.

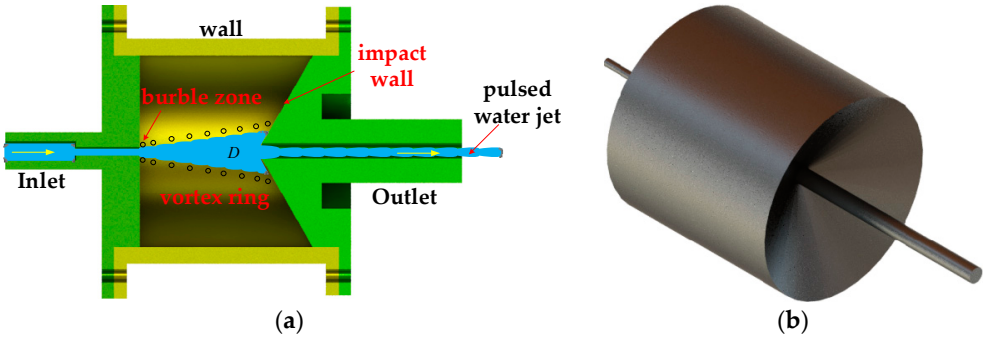

Figure 3. (**a**) Three-dimensional and (**b**) schematic diagrams of oscillating chamber.

The amplification of different frequencies by the velocity shear layer is a necessary condition for the continuous generation of the particle pulsed jet based on the latter's oscillation mechanism. The energy is continuously converted into pulse energy by constantly inducing new "pressure transients". Research has shown that the amplification of vorticity

perturbations of different frequencies by the unstable shear layer depends on the Strouhal number [34,35], whose formula is as follows:

$$S_r = \frac{fd}{U} \tag{1}$$

where f denotes the disturbance frequency [Hz]; U is jet velocity [m/s]; and d is jet diameter [m].

There must be a phase relationship between feedback and disturbance in order to generate an oscillation [36,37]. The relationship between the size of the oscillation cavity and the number of vortex rings is expressed as

$$\frac{L_D}{\varphi_1} = (N - 0.25)\frac{U_c}{U}\frac{1}{S_r(1 + Ma)} \tag{2}$$

where φ_1 is the inlet nozzle diameter [mm]; L_D is the length of the Helmholtz oscillation cavity [mm]; N is the number of vortex rings transported by the jet beam at the same time; U_c is the harmonic transport velocity [m/s]; S_r is the Strouhal number; and M_a is the Mach number.

The self-oscillating particle pulsed jet is a high-speed transient two-phase flow of water and particles. The acceleration of the particles in an oscillating water medium is considered in this paper. Since the particle concentration is less than 20%, the effect of particles on the water jet is not considered. Therefore, the motion law of a single particle is studied first, followed by the motion of the particle swarm, so as to determine the dynamic characteristics of particles in the process of applying a particle pulsed jet. Before modeling, the following assumptions were made:

(1) The heat exchange on the inner wall of the outlet of the particle pulsed jet is ignored, i.e., the particle pulsed jet exhibits one-dimensional isentropic flow in the outlet nozzle;
(2) The irregular particles are ignored, and the particles are regarded as ideal balls;
(3) The interaction between particles is ignored;
(4) The influence of outlet vibration on the particle pulsed jet is ignored;
(5) The particle pulsed jet in the outlet is approximately regarded as a heterogeneous mixed medium without a phase change.

2.1. Equation of Motion—Single Particle

First, the motion properties of individual particles are modeled. In order to facilitate simplification and calculation, the gravity, Basset force, Magnus force, Suffman force, and lift force of a single particle are ignored according to the characteristics and assumptions of the particle pulsed jet. Only the inertial force, drag force, pressure differential force, and additional mass force of a single particle are considered [38,39], so the one-dimensional equation of motion of a single particle is given as

$$\begin{cases} \frac{\pi}{6}d_s^3\rho_s\frac{du_s}{dt} = \frac{1}{2}C_s\rho_1(u_1 - u_s)|u_1 - u_s|\frac{\pi}{4}d_s^2 - \frac{\pi}{6}d_s^3\frac{dp_1}{dx} + \frac{\pi}{12}d_s^3\rho_1\left(\frac{du_1}{dt} - \frac{du_s}{dt}\right) \\ \rho_1 = \frac{m_1}{u_1 A} \\ A = \frac{\pi\varphi_2^2}{4} \end{cases} \tag{3}$$

where d_s is particle diameter [m]; u_s, u_1 are the speed of particles and water, respectively [m/s]; ρ_s and ρ_1 are the density of particles and water, respectively [kg/m^3]; m_1 is the mass flow rate of the fluid medium [kg/s]; A is the section area of the outlet nozzle [m^2]; φ_2 is the outlet nozzle's inner diameter [m]; μ_1 is the dynamic viscosity of the fluid [Pa·s]; P_1 denotes the pressure of the fluid; and C_s is the drag coefficient of the particle, which can be obtained as follows:

$$C_s = \begin{cases} \frac{24}{\mathrm{Re}_s}\left(1 + \frac{1}{6}\mathrm{Re}_s^{\frac{2}{3}}\right)(\mathrm{Re}_s \le 1000) \\ 0.424(\mathrm{Re}_s > 1000) \end{cases} \tag{4}$$

The Reynolds number of the particle Re_s is expressed as follows:

$$\mathrm{Re}_s = \frac{\rho_s d_s |u_1 - u_s|}{u_1} \tag{5}$$

The first term on the right of the first equation in Equation (3) is the friction force of the fluid medium acting on the particles, which can accelerate the particles. The second term is the influence of the fluid pressure gradient. The third term is the additional mass force, which is the effect of the mass of the loaded fluid on the particles' acceleration.

By transforming Equation (3), the following formula can be obtained:

$$\frac{du_s}{dt} = \frac{u_1 - u_s}{\tau_{cv}} + \frac{1}{2}\frac{\rho_1}{\rho_s}\frac{d(u_1 - u_s)}{dt} - \frac{1}{\rho_s}\frac{dp_1}{dx} \tag{6}$$

$$\tau_{cv} = \frac{\rho_s d_s^2}{18\mu_1} \cdot \frac{1}{C_s \frac{\mathrm{Re}_s}{24}} = \frac{\rho_s d_s^2}{18\mu_1} \cdot \frac{1}{f(\mathrm{Re}_s)} \tag{7}$$

$$t_{cv} = \frac{\rho_s d_s^2}{18\mu_1} \tag{8}$$

$$f(Re_s \mathrm{Re}_s) = \begin{cases} +\frac{1}{6}\mathrm{Re}_s^{\frac{2}{3}} (\mathrm{Re} \le 1000) \\ 0.0176\mathrm{Re}_s (Re > 1000)(\mathrm{Re} > 1000) \end{cases} \tag{9}$$

where τ_{cv} is the velocity relaxation time of a particle [s], and t_{cv} is the velocity relaxation time corresponding to stokes resistance [s].

By eliminating the pressure gradient term in Equations (6) and (9), the motion equation of a single particle can be obtained:

$$\frac{du_s}{dt} = \frac{u_1 - u_2}{\lambda_2 \tau_{cv}} + \frac{\lambda_2 - \lambda_1}{\lambda_2}\frac{du_1}{\mathrm{dt}} \tag{10}$$

$$\begin{cases} \lambda_1 = 1 - \frac{\rho_1}{\rho_s} \\ \lambda_2 = 1 + \frac{\rho_1}{2\rho_s} \end{cases} \tag{11}$$

2.2. The Equation of Motion of a Particle Swarm

Due to the large particle content involved in the rock-breaking process, there is no single particle breaking the rock. Therefore, the motion equation of a particle swarm has been established. Compared with the motion of a single particle, it is necessary to consider the change in the drag coefficient caused by the interaction between particles and the influence of the fluid on the particle swarm during the acceleration process of the particle swarm in the fluid. Among all the external forces acting on the particle, only the friction force between the particle pulsed jet flowing in the rear nozzle and the inner wall of the exit is considered [38–40]. The mass flow rate of the particle and the mass flow rate of the fluid medium on any section inside the outlet are unchanged, and the momentum equation of the fluid and particles inside the outlet is as follows:

$$\dot{m}_1 du_1 + \dot{m}_s du_s = -dF_f \tag{12}$$

$$\begin{cases} dF_f = \pi d_s dx \tau_f \\ \tau_f = C_f \frac{\rho_f u_1^2}{2} \\ \rho_f = \frac{4\dot{m}_f}{\pi u_1 d_s^2} \end{cases} \tag{13}$$

The following equation can be obtained by substituting Equation (13) into Equation (12):

$$\dot{m}_1 du_1 + \dot{m}_s du_s = -\frac{2}{d_s^2} C_f u_1^2 dt \tag{14}$$

After substituting $dx = u_1 dt$ into Equation (14), the solution can be obtained by dividing both sides by $\dot{m}_f$

$$\begin{cases} \phi_1 du_1 + \phi_s du_s = -\frac{2}{d_s^2} C_f u_1^2 dt \\ du_m = -\frac{2}{d_s^2} C_f u_1^2 dt \end{cases} \tag{15}$$

where τ_f is the frictional stress between the particle pulsed jet and the inner wall of the outlet [Pa]; ρ_f is pulsed particle jet density [kg/m^3]; ϕ_1 is the mass fraction of fluid in a particle pulsed jet, $\phi_1 = \frac{\dot{m}_1}{\dot{m}_f}$; ϕ_s is the mass fraction of a particle in a particle pulsed jet, $\phi_s = \frac{\dot{m}_1}{\dot{m}_f}$; $\dot{m}_s$ is the particle mass flow rate [kg/s]; $\dot{m}_f$ is the particle pulsed jet mass flow rate [kg/s]; u_m is the instantaneous convergence rate of fluid and particles [m/s].

$$u_m = \phi_1 u_1 + \phi_s u_s \tag{16}$$

By substituting Equation (16) into Equation (10), the motion equation of particles in the particle swarm can be obtained as follows:

$$\begin{cases} \frac{du_s}{dt} = \frac{u_m - u_s}{\lambda_2 \phi_1 \tau_v} + \frac{\lambda_2 - \lambda_1}{s_2} \frac{du_1}{dt} \\ \tau_v = \frac{\tau_0}{\frac{C_s Re_s}{24}} \\ \tau_0 = \frac{\rho_s d_s^2}{18 \mu_f} \end{cases} \tag{17}$$

where τ_v is the velocity relaxation time of a particle swarm [s]; τ_0 is the velocity relaxation time corresponding to Stokes resistance [s]; and μ_f is the equivalent dynamic viscosity of a solid–liquid mixed medium. The following can be obtained by applying Einstein equation:

$$\mu_f = \mu_1 (1 + 2.5 \alpha_s) \tag{18}$$

where μ_1 is the viscosity of water, and α_s is the volume fraction of a particle.

2.3. Equation of Particle Motion in a Particle Pulsed Jet

The flow of the particle pulsed jet at the outlet is considered to be a first-order main frequency oscillation. Consequently, Equation (17) can be simplified as follows:

$$\frac{du_s}{dt} = \frac{u_1 - u_s}{\lambda_2 \phi_1 \tau_{fv}} + \frac{\lambda_2 - \lambda_1}{\lambda_2} \frac{du_1}{dt} \tag{19}$$

After the particle jet enters the oscillating chamber, it oscillates, and the particles gain higher kinetic energy under the acceleration of the pulsed water jet effect. The velocity of the mixed jet is regarded as the synthesis of the average velocity and the pulse velocity, which is simplified using a Fourier series, as follows:

$$u_1 = \overline{u}_1 + \widetilde{u}_{Ai} \sin(\omega t + \varepsilon_i) \tag{20}$$

where u_1 is the velocity of the mixed jet [m/s]; $\widetilde{u}_{\mathrm{Ai}}$ is the maximum amplitude of the i-order oscillation; $\overline{u}_1$ is the average velocity of a fluid [m/s]; ω is the vibration angular frequency, $\omega = 2\pi f$; and ε_i is the first phase of the order i [rad].

By substituting Equation (20) into Equation (19), the following equation can be obtained:

$$\frac{du_s}{\mathrm{dt}} = \frac{\overline{u}_1 - u_s}{\lambda_2 \varepsilon_1 \widetilde{\tau}_v} + \frac{\widetilde{u}_{1A}}{\widetilde{\tau}_v} \cos(\omega t + \varepsilon_1 + \Phi) \tag{21}$$

where

$$\begin{cases} \widetilde{u}_{1A} = \xi \widetilde{u}_{A1} \\ \xi = \sqrt{1 + [(\lambda_2 - \lambda_1)\omega\tau_v]^2} \\ \cos\varepsilon_1 = \frac{1}{\xi} \\ \sin\varepsilon_1 = \frac{(\lambda_2 - \lambda_1)\omega\tau_v}{\xi} \\ \widetilde{\tau}_v = \lambda_2 \tau_v \end{cases} \tag{22}$$

The approximate expression of particle velocity obtained by solving Equation (22) is as follows:

$$u_s = \overline{u}_s + \widetilde{u}_{sA} \cos(\omega t + \psi) + (\widetilde{u}_{s0} - \widetilde{u}_{sA} \cos\psi) \exp\left(\frac{-t}{\lambda_2 \tau_v}\right) \tag{23}$$

where

$$\begin{cases} \widetilde{u}_{SA} = \frac{\xi}{\eta} \widetilde{u}_{A1} \\ \eta = \sqrt{1 + (\lambda_2 \omega \tau_v)^2} \\ \psi = \varepsilon + \varepsilon_1 + \varepsilon_2 \\ \cos\varepsilon_2 = \frac{1}{\eta} \\ \sin\varepsilon_2 = \frac{-\lambda_2 \omega \tau_v}{\eta} \\ \psi - \varepsilon = \varepsilon_1 + \varepsilon_2 = -\arctan\left[\frac{\lambda_1 \omega \tau_v}{1 + \lambda_2(\lambda_2 - \lambda_1)\omega^2 \tau_v^2}\right] \end{cases} \tag{24}$$

where $\overline{u}_s$ is the average velocity of particle motion [m/s]; $\widetilde{u}_{SA}$ is the amplitude of the particle pulsation velocity [m/s]; ψ is the phase angle of the particle pulsation velocity [rad]; and $\widetilde{u}_{S0}$ is the difference between a particle's initial velocity and its average velocity [m/s].

As shown in Equation (23), particle velocity consists of three parts: average velocity, based on which particles pulsate; the oscillation velocity; and the attenuation part of the particle velocity. When the pulse gradually becomes stable, the term is zero. Therefore, Equation (23) can be simplified as

$$u_s = \overline{u}_s + \widetilde{u}_{sA} \cos(\omega t + \psi) \tag{25}$$

2.4. Smooth Particle Dynamics Coupled with Finite Element Method

In the numerical simulation process, problems such as a high strain of rock fragmentation and a large deformation of a jet occur. Although finite element methods (FEMs), such as Eulerian or Lagrangian methods, have good computational accuracy, they may suffer from calculation termination due to grid distortion when dealing with large deformation. Although the smooth particle dynamics method (SPH) may not have the same computational accuracy as the FEM method, it has a wide range of applications in the field of impact collision and stress wave failure due to its lack of grid elements, strong adaptability, and ability to be quickly calculated [41]. In the process of a particle pulsed jet impinging on rock, if the high-speed pulsed water jet, particle flow, and rock are modeled using the SPH method, the calculation cost is greatly increased. If the finite element method is used for modeling, the rheology of a high-pressure water jet and particle flow cannot be simulated effectively. Based on the above considerations, the SPH method was used to model a high-pressure pulsed water jet and particle flow, while the finite element method (FEM) was used to model rock [40,42].

As shown in Figure 4, the position coordinates and velocity coordinates of the element nodes at the coupling interface are (x_F, y_F, z_F) and (u_F, v_F, w_F). The position coordinates

and velocity of each node are equivalent to SPH virtual particles with definite position and velocity. The equivalent coordinates are as follows:

$$\begin{cases} x_{\mathrm{SPH}} = \frac{1}{N}\sum_{j=1}^{N} x_F \\ y_{\mathrm{SPH}} = \frac{1}{N}\sum_{j=1}^{N} y_F \\ z_{\mathrm{SPH}} = \frac{1}{N}\sum_{j=1}^{N} z_F \end{cases} \tag{26}$$

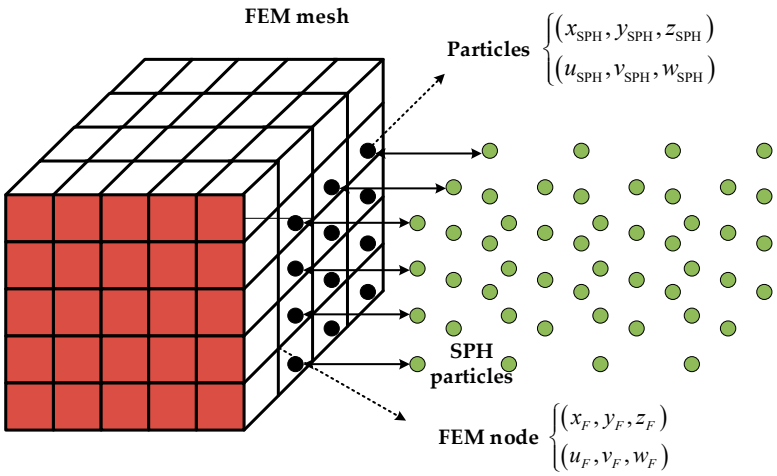

Figure 4. Basic principle of SPH-FEM coupling algorithm.

The equivalent velocities in the last three directions are

$$\begin{cases} u_{\mathrm{SPH}} = \frac{1}{N}\sum_{j=1}^{N} u_F \\ v_{\mathrm{SPH}} = \frac{1}{N}\sum_{j=1}^{N} v_F \\ w_{\mathrm{SPH}} = \frac{1}{N}\sum_{j=1}^{N} w_F \end{cases} \tag{27}$$

where N is the number of FEM mesh nodes.

The virtual particles and SPH particles at the coupling interface are calculated using the "contact algorithm based on Riemannian solution", and the velocities of the virtual particles and SPH particles on both sides of the coupling interface are projected onto the Central Line of the two particles, respectively. Then, the velocity projection of the two particles on the Central Line between them is expresses as

$$\begin{cases} v_{iSPH} = \frac{u_{iSPH}(x_j - x_{iSPH}) + v_{iSPH}(y_j - y_{iSPH}) + w_{iSPH}(z_j - z_{iSPH})}{d_{ijSPH}} \\ v_j = \frac{u_j(x_j - x_{iSPH}) + v_j(y_j - y_{iSPH}) + w_j(z_j - z_{iSPH})}{d_{ijSPH}} \end{cases} \tag{28}$$

The distance between particle i and j can be given as

$$d_{ijSPH} = \sqrt{(x_j - x_{iSPH})^2 + (y_j - y_{iSPH})^2 + (z_j - z_{iSPH})^2} \tag{29}$$

The velocity, density, and pressure of particles on both sides of the interface are $(v_{iSPH}, \rho_{iSPH}, p_{iSPH})$ and (v_j, ρ_j, p_j), respectively. The speed of sound in the two media is (c_{iSPH}, c_j). Then, the velocity and pressure on the contact surface are solved using the Riemann solver, as follows:

$$\begin{cases} v_{ij} = \frac{\rho_{iSPH} c_{iSPH} v_{iSPH} + \rho_j c_j v_j + (p_{iSPH} - p_j)}{\rho_{iSPH} c_{iSPH} + \rho_j c_j} \\ p_{ijSPH} = \frac{\rho_{iSPH} c_{iSPH} p_j + \rho_j c_j p_{iSPH} - \rho_{iSPH} c_{iSPH} \rho_j c_j (v_j - v_{iSPH})}{\rho_{iSPH} c_{iSPH} + \rho_j c_j} \end{cases} \tag{30}$$

When coupling is carried out, the position and velocity of virtual particles at the coupling point are updated according to Equations (26) and (27). The element pressure on the finite element grid at the coupling interface is obtained from the average SPH particle pressure near the element center.

3. Experimental Research

The rock-breaking theory of a particle pulsed jet was studied by means of the self-developed experimental device of particle pulsed jet impact rock breaking.

The experimental system can be divided into seven main parts according to the key experimental components: a pump, a particle injection system, a simulated top drive, a simulated bottom hole device, a high-pressure manifold, a particle storage tank, and a circulating water tank. The system's specific layout scheme and physical components are shown in Figure 5.

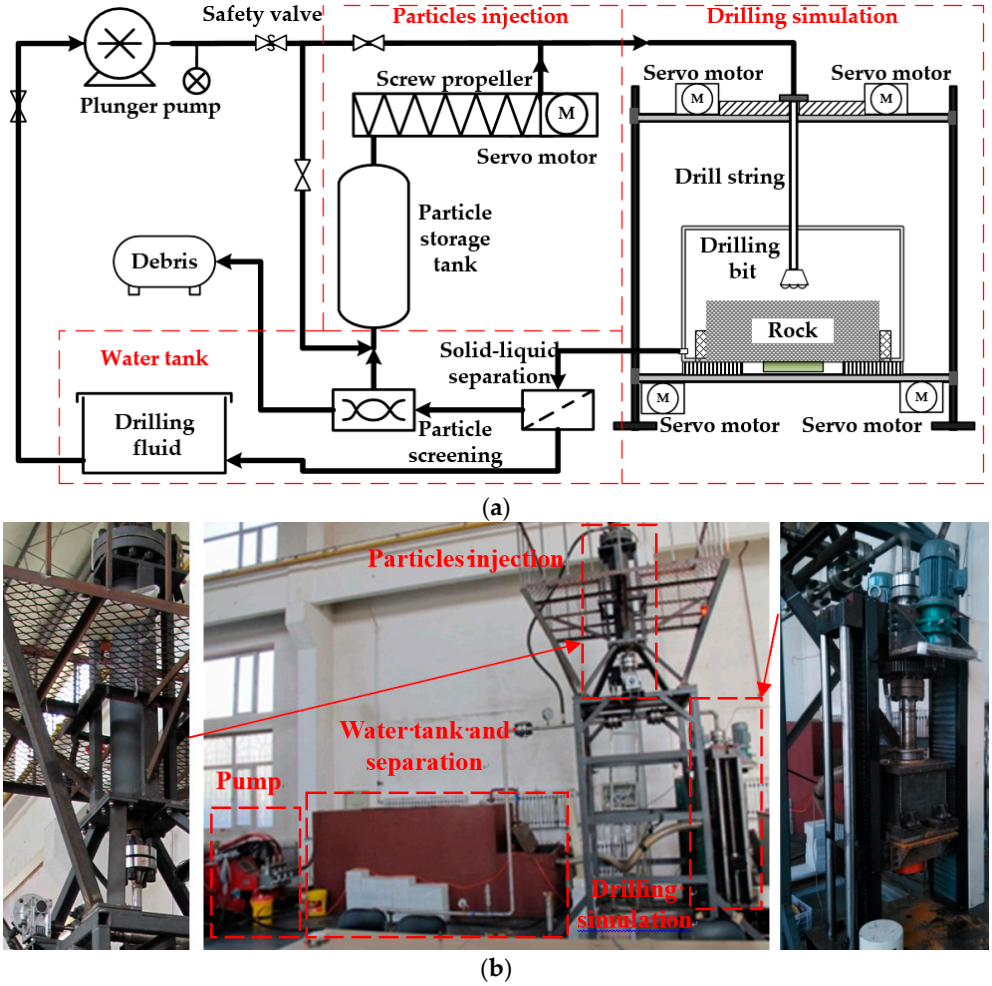

Figure 5. Experimental apparatus for rock breaking via particle pulsed jet impact: (**a**) layout scheme; (**b**) the actual structure of the experimental apparatus.

The rock used in the experiment was granite, and the experimental particles were steel particles with a diameter of 1 mm. The experimental materials are shown in Figure 6.

(**a**) (**b**)

Figure 6. Experimental materials: (**a**) rock; (**b**) particles.

For the rock parameters test, elastic modulus and Poisson's ratio testing were conducted using the dynamic elastic modulus tester, which uses the pulse excitation method for non-destructive testing. The confining pressure strength test was conducted using a triaxial tester, and when the confining pressure was 4 MPa, 8 MPa, and 12 MPa, the failure strength was about 129 MPa, 199 MPa, and 272 MPa. The tensile strength test was conducted using a universal testing machine for tensile strength testing.

4. Results and Discussion

4.1. Effect of Particle Concentration on Rock-Breaking Efficiency of Particle Pulsed Jet

In this paper, rock-breaking efficiency is used as the criterion for measuring the rock-breaking effect of particle pulsed jet, and rock-breaking efficiency is measured according to the mass of the broken rock. The rock-breaking efficiency η of the particle pulsed jet is defined as follows:

$$\eta = \frac{m_0}{M} \tag{31}$$

where m_0 is the reduction in rock mass over the entire impact process [kg], and M is the mass of a single rock sample [kg].

The numerical model of particle pulsed jet impact rock breaking is shown in Figure 7. The "segmented" modeling method was adopted in order to simulate the pulsed water and particles. The diameter of the water column was 24 mm, and its height was 60 mm, and these measurements were divided into 20 parts. Each section has a different impact speed.

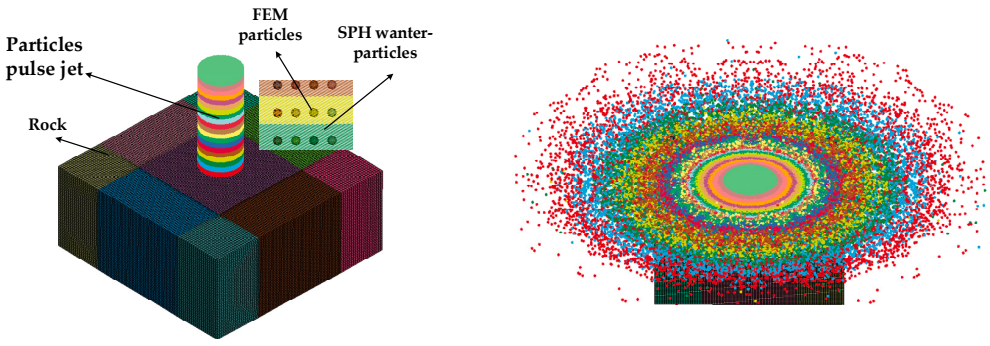

(**a**) (**b**)

Figure 7. Numerical model and splashing effect of particle pulsed jet impact on rock: (**a**) numerical model of particle pulsed jet; (**b**) the effect of particle pulsed jets on rock splashing.

The characteristics of rock are described using the Lagrangian method, and the local area is meshed during modeling. The mesh size of the dense area is 0.5 mm, and the independence of the mesh is shown in Figure 8. The entire rock mass is divided into 1,000,000 grids.

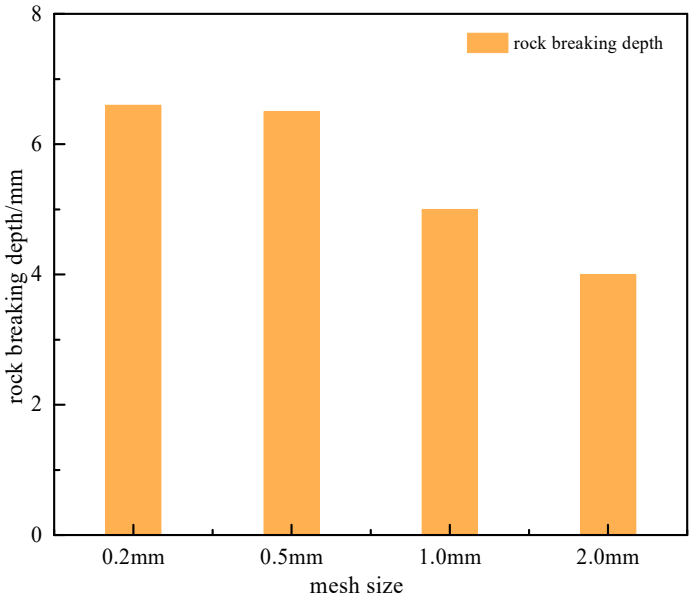

Figure 8. Independency analysis under different mesh sizes.

In the process of the particle pulsed jet impacting the rock, the particle concentration, the average particle velocity, and the width of the water jet will affect the rock-breaking efficiency. The "piecewise modeling method" and the "SPH-FEM" coupling method were used to analyze the influence of the above factors on the rock-breaking efficiency, laying a theoretical foundation for the subsequent particle pulsed jet impact on rock breaking. On the premise that the average velocity and variance of the particle pulsed jet impacting the rock are consistent, the particle concentrations were changed to 0.0375%, 0.15%, and 0.3%. The results of rock breaking are shown in Figure 9, in which the different rock-breaking efficiency values are compared. With the increase in particle concentration, the rock-breaking efficiency of the particle pulsed jet also increases. When the particle concentration increases from 0.15% to 0.3%, the increase in rock-breaking efficiency is basically the same as the change in the rock-breaking efficiency when the particle concentration increases from 0.0375% to 0.15%, so it can be surmised that there is an optimal rock-breaking efficiency value for particle concentration. When the particle concentration is too high, the impact of the particles on the rock could be affected by the collision between the particles, and the wear of the drill would be aggravated.

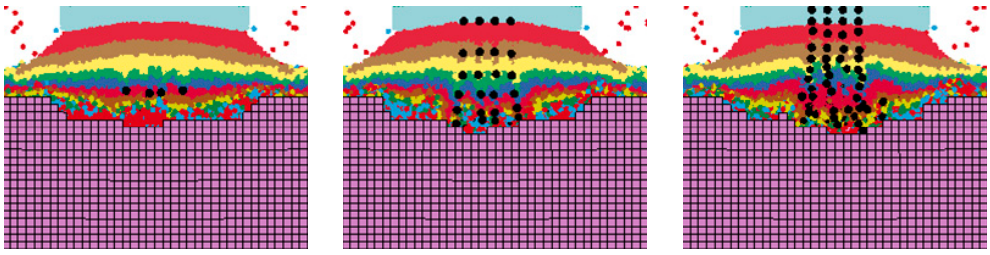

Figure 9. Impact of pulsed jets of different particle concentrations on rock: (**a**) 0.0375%; (**b**) 0.15%; (**c**) 0.3%.

Due to the complex conditions during the test, the characteristics of the rock were also unstable. In this study, several experiments were conducted with the same parameters, and these parameters are shown in Table 2. Ten experiments were carried out with the particle concentrations of 0.0375%, 0.15%, and 0.3%. The results obtained in the experiment are shown in Figure 10, and the statistical results of the experiments are shown in Figure 11.

Table 2. Parameters employed in this paper.

Particle Concentration	Particle Diameter	Injection Angle	Time
0.0375%, 0.15%, 0.3%	1 mm	90°	10 s

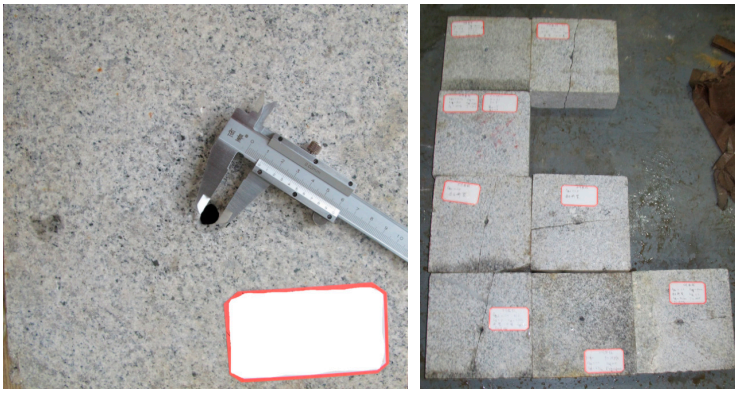

Figure 10. Experimental samples.

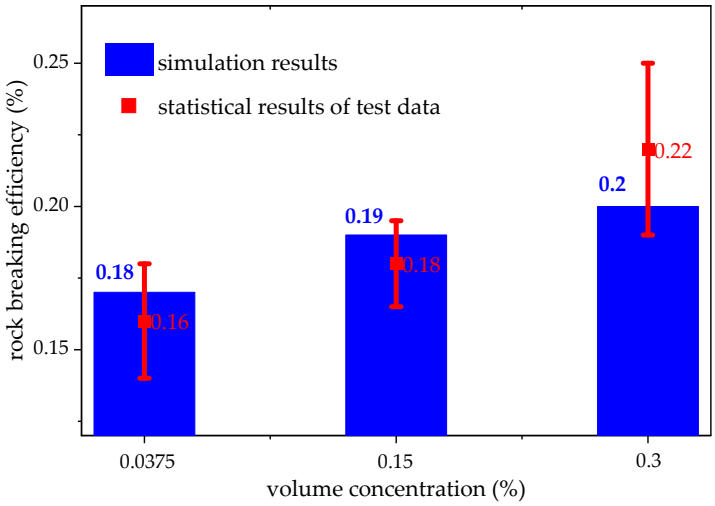

Figure 11. Statistical results of experiment and simulation.

When the particle concentration was 0.0375%, the rock-breaking efficiency values were 0.14–0.18%, and the average value of the multiple experiments was 0.16%. When the particle concentration was 0.15, the average rock-breaking efficiency was 0.18%. The rock-breaking efficiency ranged from 0.18 ± 0.015%. When the particle concentration was 0.3%, the average rock-breaking efficiency increased to 0.22%, and the maximum rock-breaking efficiency was 0.25%. It can be seen from the simulation and experimental results that rock-breaking efficiency shows an upward trend with the increase in the particle concentration, and the simulated rock-breaking efficiency increases from 0.18% to 0.2%, with an increment of 0.02%. The experimental rock-breaking efficiency increased from 0.16% to 0.22%, with an increment of 0.06%. Although the experimental improvement is larger, its behavior is consistent with the simulation, showing a gradual improvement trend. The errors between the experiments and simulation are 11%, 5%, and 9%, respectively. These errors are within the allowable range. The performance of many experiments proved the accuracy of the simulation results and mathematical models.

4.2. Effect of Average Velocity of Particle Pulsed Jet on Rock-Breaking Efficiency

The average velocity of the particle pulsed jet reflects the energy spent when it breaks rock. The rock-breaking efficiency of the particle pulsed jet with average velocities of

133 m/s, 161 m/s, and 170 m/s was studied based on the modeling method and coupling method mentioned above, as shown in Figure 11. In general, the impact of rock-breaking efficiency increases with the improvement of the average velocity of the particle pulsed jet. However, when the average speed exceeds 161 m/s, the growth rate of the rock-breaking efficiency suddenly increases. By comparing Figure 12a–c, it can be found that when the average jet velocity is 170 m/s, the distribution of particle impacts on the rock is more concentrated, and the rock-breaking depth increases more markedly.

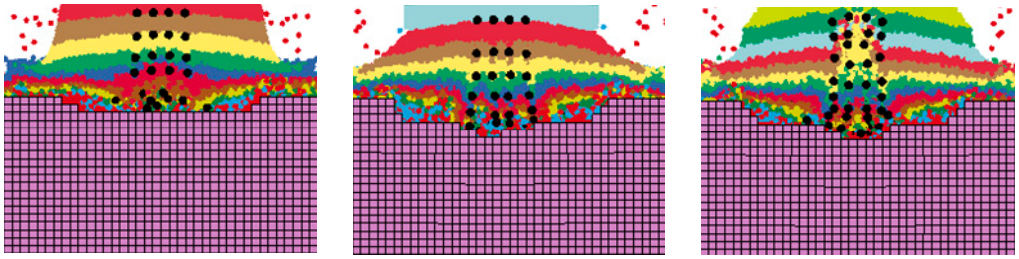

(**a**) (**b**) (**c**)

Figure 12. The impact of pulsed jet of particles with different average velocities on the rock: (**a**) 133 m/s; (**b**) 161 m/s; (**c**) 170 m/s.

Then, the simulation of different jet velocities was verified through multiple experiments, and the parameters used are shown in Table 3:

Table 3. Parameters applied in this paper.

Particle Speed	Particle Concentration	Particle Diameter	Injection Angle	Time
133 m/s, 161 m/s, 170 m/s	0.15%	1 mm	90°	10 s

The rock-breaking efficiency results of the simulation and experiments are shown in Figure 13. The simulation results show that when the particle velocity was 133 m/s, 161 m/s, and 170 m/s, the corresponding rock-breaking efficiency was 0.089%, 0.19%, and 0.214%, respectively. With the increase in particle velocity, the rock-breaking efficiency is greatly improved. A large number of experiments have also been carried out with the parameters adopted in the simulation (experimental parameters are shown in Table 3). The experimental results show that when the speed was 133 m/s, the average rock-breaking efficiency was 0.11%, and the maximum test efficiency was 0.13%. When the speed was 161 m/s, the rock-breaking efficiency significantly increased to 0.18%, an increment of 38%, and the highest efficiency was 0.195%. When the particle velocity was 170 m/s, the rock-breaking efficiency fluctuated between 0.205 and 0.265%. It can be seen from the simulation and experimental results that the rock-breaking efficiency increases with the improvement of the particle velocity, and their trends are consistent. The error values of the test and simulation under the three parameters were 19%, 5%, and 9%, respectively. Because the assumptions of the test and simulation are slightly different, the error of the results is within the acceptable range. The simulation and experiments have been mutually verified. The mathematical model established in this paper accurately reflects the whole process of particle pulsed jet rock breaking.

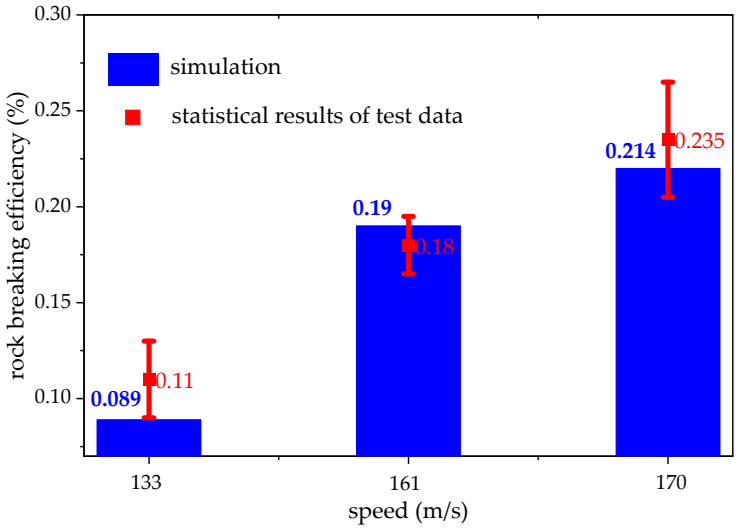

Figure 13. The rock-breaking efficiency varies with the impact velocity of the particle jet.

4.3. Advantages and Applications of This Research

The particle pulsed jet rock-breaking technology combines the advantages of particle impact drilling and pulsed jet rock-breaking technology. Since it does not alter the traditional drilling equipment and processes, the non-contact rock breaking process of high-speed particle and pulsed jet rock breaking can not only improve drilling speed but also purify the bottom hole flow field and ameliorate the repeated wear of the particle rock-breaking bit. The technical advantages of this method are as follows: (1) there is no need to change the existing drilling equipment and drilling process, and a frequency-adjustable particle pulsed jet rock-breaking device can be directly connected to the underground system; (2) the particles and drilling fluid are modulated and accelerated to form a high-frequency, high-speed, and pulsating particle jet, allowing for the rapid fragmentation of hard rock layers; (3) rocks can be easily crushed with lower bit pressure and torque, thereby reducing wellbore deviation and downhole accidents; and (4) a pulsed jet can pulsate and enhance characteristics, clean and purify rock debris and particles in the wellbore flow field, and improve the return efficiency of particles and debris.

The particle pulsed jet technology and simulation method proposed in this article can be applied to related fields such as oil drilling, cutting, mining, etc. For particles, abrasives of different shapes and materials can be considered and changed according to the application scenario.

5. Conclusions

As a new drilling technology based on particle jets and a high-pressure pulsed jet, particle jet impact rock-breaking technology has great application prospects. In this paper, numerical simulation and experimental research were used to verify the results. The conclusions of this paper are as follows:

(1) When the variance is constant, the rock-breaking efficiency increases with the increase in the average particle pulsed jet velocity, and the impact rock-breaking efficiency also increases. When the speed reaches 133 m/s, the rock-breaking efficiency is low, amounting to 0.089%. When the average speed exceeds 160 m/s, the growth rate of the rock-breaking efficiency suddenly increases significantly by 113%, and the rock-breaking efficiency jumps to 0.18%. With the increasing speed, the efficiency of rock breaking is limited. When the speed is increased to 170 m/s, the rock-breaking efficiency reaches 0.214%. As the speed continues to increase, the efficiency of rock breaking deteriorates.

(2) With the increase in particle concentration, the rock-breaking efficiency of the particle pulsed jet also increases. When the particle concentration increases from 0.15% to

0.3%, the increase in rock-breaking efficiency is basically consistent with the change in rock-breaking efficiency when the particle concentration increases from 0.0375% to 0.15%, and the final simulated rock-breaking efficiency reaches 0.2%. At the same time, the trends of the experimental results and simulation are the same. When the concentrations are 0.0375%, 0.15%, and 0.3%, the error values of the simulation and test are 11%, 5.3%, and 10%, respectively, and these error values are within the allowable range. These two test methods have confirmed the accuracy of our results. Therefore, it can be surmised that there is an optimal rock-breaking efficiency value in relation to particle concentration. When the particle concentration is too high, the collision between particles affects the impact of the particles on the rock and will aggravate the wear of the drill bit; thus, a high concentration of particles should not be the goal.

Author Contributions: Conceptualization, X.Y. and H.S.; methodology, T.F.; software T.Z.; validation, H.L. and T.Z.; formal analysis, T.F.; investigation, T.F.; resources, Q.W.; data curation, T.Z.; writing—original draft preparation, T.F. and H.S.; writing—review and editing, T.F. and T.Z.; visualization, H.L.; supervision, X.Y. and Q.W.; project administration, X.Y. and Q.W. All authors have read and agreed to the published version of the manuscript.

Funding: This study was funded by the National Natural Science Foundation of China (11972113), the Guiding Innovation Fund Project of Northeast Petroleum University (2019YDL-07), and the Natural Science Foundation of Heilongjiang Province (LH2023A002).

Institutional Review Board Statement: Not applicable.

Informed Consent Statement: Not applicable.

Data Availability Statement: Data are unavailable due to privacy concerns.

Conflicts of Interest: The authors declare no conflict of interest.

References

1. Fang, T.; Ren, F.; Liu, H.; Zhang, Y.; Cheng, J. Progress and development of particle jet drilling speed increasing technology and rock-breaking mechanism for deep well. *J. Pet. Explor. Prod. Technol.* **2022**, *12*, 1697–1708. [CrossRef]
2. Abdelghany, W.K.; Radwan, A.E.; Elkhawaga, M.A.; Wood, D.A.; Sen, S.; Kassem, A.A. Geomechanical Modeling Using the Depth-of-Damage Approach to Achieve Successful Underbalanced Drilling in the Gulf of Suez Rift Basin. *J. Pet. Sci. Eng.* **2021**, *202*, 108311. [CrossRef]
3. Yang, M.; Yang, Y.; Bian, W.; Wu, J. Drilling progress and technological improvement of ultradeep wells in Russia. *Oil Drill. Prod. Technol.* **2021**, *43*, 15–20. [CrossRef]
4. Zhang, B.; Lu, N.; Guo, Y.; Wang, Q.; Cai, M.; Lou, E. Modeling and Analysis of Sustained Annular Pressure and Gas Accumulation Caused by Tubing Integrity Failure in the Production Process of Deep Natural Gas Wells. *J. Energy Resour. Technol. Trans.* **2022**, *144*, 063005. [CrossRef]
5. Li, D.; He, D.; Santosh, M.; Ma, D.; Tang, J. Tectonic framework of the northern Junggar Basin Part I: The eastern Luliang Uplift and its link with the East Junggar terrane. *Gondwana Res.* **2015**, *27*, 1089–1109. [CrossRef]
6. Liu, W.; Xi, Y.; Cha, Q.; Guo, Q.; Xu, C.; Wang, W. Study on Penetration Depth and Rock Breaking Mechanism of PDC Cutter in Different Percussion DrillingMethods. *Xinjiang Oil Gas* **2023**, *19*, 17–23.
7. Liu, F.; Sun, J.; Wang, J. A Global Review of Technical Status and Development Trend of Drilling Fluids for Deep and Ultra-Deep Wells. *Xinjiang Oil Gas* **2023**, *19*, 34–39.
8. Wang, B.; Wang, L.; Liu, X.; Ren, F. Bifurcation Diagram and Dynamic Response of a Drill String Applied in NGH Drilling. *Processes* **2022**, *10*, 1111. [CrossRef]
9. Bondarenko, N.A. ISM High-Performance Tools for Drilling of Oil and Gas Wells. *Rev. J. Superhard Mater.* **2018**, *40*, 355–364. [CrossRef]
10. Stuart, D.C.W.; Daniel, V. Simulating electropulse fracture of granitic rock. *Int. J. Rock Mech. Min. Sci.* **2020**, *128*, 104238. [CrossRef]
11. Akhter, M.; Mallams, J.; Tang, X.; Staack, D. Underwater plasma breakdown characteristics with respect to highly pressurized drilling applications. *J. Appl. Phys.* **2021**, *129*, 183309. [CrossRef]
12. Hou, Y.; Qi, S.; You, H.; Huang, Z.; Niu, Q. The study on pyrolysis of oil-based drilling cuttings by microwave and electric heating. *J. Environ. Manag.* **2018**, *228*, 312–318. [CrossRef]

13. Deyab, S.M.; Rafezi, H.; Hassani, F.; Kermani, M.; Sasmito, A.P. Experimental investigation on the effects of microwave irradiation on kimberlite and granite rocks. *J. Rock Mech. Geotech. Eng.* **2021**, *13*, 267–274. [CrossRef]
14. Liang, D.; Guan, Z.; Wang, J.; Tao, X. Simulation Analysis of Drilling Process in Horizontal Wells with Mechanical Rotary Percussion Tool. *Chem. Technol. Fuels Oils* **2022**, *58*, 114–121. [CrossRef]
15. Zhang, X.; Yi, M.; Qiao, D.; Wang, W.; Li, F. Application of studying the effect of mechanical rotary drilling. *Xinjiang Oil Gas* **2019**, *15*, 79–82.
16. Zhang, S.; Huang, J.; Miao, X.; Zhan, H.; Liang, H.; Zhao, K. Characterizing the laser drilling process of oil shale using laser-induced voltage. *Opt. Laser Technol.* **2020**, *131*, 106478. [CrossRef]
17. Jamali, S.; Wittig, V.; Börner, J.; Bracke, R.; Ostendorf, A. Application of high powered Laser Technology to alter hard rock properties towards lower strength materials for more efficient drilling, mining, and Geothermal Energy production. *Geomech. Energy Environ.* **2019**, *20*, 100112. [CrossRef]
18. Jin, X.M.; Huang, Y.Y.; Yuan, Z.T.; Dong, M.; Jiang, X. Research progress and application prospects of new methods for efficient rock breaking. *Petrochem. Ind. Appl.* **2019**, *38*, 1–6.
19. Lu, Y.; Huang, F.; Liu, X.; Ao, X. On the failure pattern of sandstone impacted by high-velocity water jet. *Int. J. Impact Eng.* **2015**, *76*, 67–74. [CrossRef]
20. Yuan, M.; Li, D.; Kang, Y.; Shi, H.; Pan, H. Characteristics of Oscillation in Cavity of Helmholtz Nozzle Generating Self-excited Pulsed Waterjet. *Chin. J. Mech. Eng.* **2022**, *35*, 73. [CrossRef]
21. Zhu, X.H.; He, L.; Liu, W.J.; Wang, S.; Luo, Y. The Mechanism of Particle Impact-Assisted Rock Cutting in Hard Brittle Granite. *Arab. J. Sci. Eng.* **2022**, *47*, 11915–11928. [CrossRef]
22. Huang, F.; Zhao, Z.; Li, D.; Mi, J.; Wang, R. Investigation of the breaking manifestations of bedded shale impacted by a high-pressure abrasive water jet. *Powder Technol.* **2022**, *397*, 117021. [CrossRef]
23. Dhakal, H.N.; Ismail, S.O.; Ojo, S.O.; Paggi, M.; Smith, J.R. Abrasive water jet drilling of advanced sustainable bio-fibre-reinforced polymer/hybrid composites: A comprehensive analysis of machining-induced damage responses. *Int. J. Adv. Manuf. Technol.* **2018**, *99*, 2833–2847. [CrossRef]
24. Thomas, H. Particle Drilling Pulverizes Hard Rocks. *Am. Oil Gas Report.* **2007**, *50*, 86–89.
25. Momber, A.W. The response of geo-materials to high-speed liquid drop impact. *Int. J. Impact Eng.* **2016**, *89*, 83–101. [CrossRef]
26. Zhao, J.; Han, L.X.; Xu, Y.J.; Jin, J.; Liu, F. Theory and on-site testing of particle impact drilling technology. *Nat. Gas Ind.* **2014**, *34*, 102–107.
27. Rach, N.M. Particle-impact drilling blasts away hard rock. *Oil Gas J.* **2007**, *105*, 43–48.
28. Foreman, S.E.; Secor, G.A. The mechanics of rock failure due to water jet impact. Sixth Conference on Drilling and Rock Mechanics. *Soc. Pet. Eng.* **1974**, *14*, 10–18. [CrossRef]
29. Ai, H.A.; Ahrens, T.J. Simulation of Dynamic Response of Granite: A numerical Approach of Shock-induced Damage Beneath Impact Craters. *Int. J. Impact Eng.* **2006**, *33*, 1–10. [CrossRef]
30. Cheng, X.Z. Numerical Analysis and Experimental Study on Rock Breaking by Particle-Jet Coupled Impact. Ph.D. Thesis, Northeast Petroleum University, Daqing, China, 2018.
31. Ren, F.; Fang, T.; Cheng, X.; Cheng, J. Failure volume under particle water-jet impact in deep well drilling engineering: Mathematical modeling and verification analysis. *Alex. Eng. J.* **2021**, *60*, 1839–1849. [CrossRef]
32. Ren, F.S.; Fang, T.C.; Cheng, X.Z. Theoretical modeling and experimental study of rock-breaking depth in particle jet impact drilling process. *J. Pet. Sci. Eng.* **2019**, *183*, 106419. [CrossRef]
33. Ren, F.S.; Fang, T.C.; Cheng, X.Z. Study on rock damage and failure depth under particle water-jet coupling impact. *Int. J. Impact Eng.* **2020**, *139*, 103504. [CrossRef]
34. Deng, Q.; Zhou, H.; Lv, B.; Wang, Y.; Yuan, J.; Lou, F. Research on fluid pulse characteristics based on dual self-excited oscillation chamber abrasive flow polishing. *Surf. Technol.* **2021**, *50*, 371–379. [CrossRef]
35. Liu, W.; Kang, Y.; Zhang, M.; Wang, X.; Li, D. Self-sustained oscillation and cavitation characteristics of a jet in a Helmholtz resonator. *Int. J. Heat Fluid Flow* **2017**, *68*, 158–172. [CrossRef]
36. Wu, R.; Yang, F.; Pei, K.; Pan, Y. Optimization of self excited oscillation pulse nozzle structure based on multi-objective particle swarm optimization algorithm. *Coal Min. Mach.* **2022**, *43*, 114–116. [CrossRef]
37. Ge, Z.; Ling, Y.; Tang, J.; Lu, Y.; Zhang, Y.; Wang, L.; Yao, Q. The formation principle and characteristics of self-supercharging pulsed water jet. *Chin. J. Mech. Eng.* **2020**, *35*, 51. [CrossRef]
38. Liu, C.X.; Ma, D.P. *Advanced Rock Mechanics*; Yellow River Water Conservancy Publishing House: Zhengzhou, China, 2017.
39. Ren, F.S.; Fang, T.C.; Cheng, X.Z. Parameter optimization and experimental study of particle jet impact rock breaking nozzle. *Pet. Mach.* **2018**, *46*, 5–11. [CrossRef]
40. Li, H.; Liu, S.; Jia, J.; Wang, F.; Guo, C. Numerical simulation of rock-breaking under the impact load of self-excited oscillating pulsed waterjet. *Tunn. Undergr. Space Technol.* **2020**, *96*, 103179. [CrossRef]

41. Yu, R.; Dong, X.; Li, Z.; Fan, M. A coupled SPH–DEM model for erosion process of solid surface by abrasive water-jet impact. *Comp. Part. Mech.* **2023**, *10*, 1093–1112. [CrossRef]
42. Liu, X.; Tang, P.; Geng, Q.; Wang, X. Effect of Abrasive Concentration on Impact Performance of Abrasive Water Jet Crushing Concrete. *Shock Vib.* **2019**, *2019*, 3285150. [CrossRef]